Analytical Modeling of Oxidizer Motion and Fuel Regression in Hybrid Rockets for In-Flight Mass Evolution

Ben Virtucio,* Michael Swoyer,† Anyi X. Lin,‡ Jack R. Rumpf,* Aiden Zeng†, Harsh Patel†, Tanvi Cheruki†, Yoyi L. Xie *, Ashlyn Oritiona †, Samuel Lippencott †

Hybrid rockets experience continuous internal mass redistribution due to solid-fuel regression and propellant motion during flight. Tracking the combined influence of these effects requires modeling approaches that represent in-flight internal mass behavior. This paper focuses on the development of in-flight analytical approximations for modeling the internal mass evolution of hybrid rockets, including oxidizer drain, solid-fuel regression, and oxidizer sloshing. Oxidizer drain is modeled using a non-homogeneous, non-equilibrium mass flow rate model (Dyer) across the feed system to capture two-phase outflow as the tank empties. Solid-fuel regression is modeled using a mass-flux approach that directly relates the fuel burn rate to oxidizer flow and grain geometry. Oxidizer slosh is represented with a Duffing model coupled to vehicle accelerations. This approach enables a reduced-order, computationally efficient prediction of evolving mass properties suitable for system-level simulation throughout the burn. The aforementioned models are then combined to create a dynamics model that outputs the rocket's state in real time without resolving full fluid flow or combustion physics. In this study, thrust and wind-induced disturbances are applied to the vehicle's immediate state to stimulate response. Results demonstrate continuous updates of in-flight mass properties, with evaluation focused on mass and inertia evolution, computational performance, sensitivity to oxidizer flow, and acceleration inputs, with the validity of the model to be later examined against future tethered flight profiles.

I. Introduction

Hybrid rocket propulsion systems exhibit inherently time-varying internal mass distributions due constant propellant motion within partially filled tanks [1–3]. As the burn progresses, evolving grain geometry and fluid configuration continuously alter both the magnitude and spatial distribution of propellant mass. This shifts the vehicle of center-of-mass (COM) and moment-of-inertia (MOI) [4–6], significantly affecting stability margins and control authority depend directly on real-time mass property evolution [7, 8].

In traditional hybrid rocket analyses, oxidizer drainage, solid-fuel regression, and propellant sloshing are typically modeled independently using high-fideility CFD and multiphysics[1, 2, 5, 9–13]. This calls forth a unified, computationally efficient framework that enables continuous control updates from the simultaneous, combined dynamics to update the total mass, center of mass, and inertia properties during flight. This study presents such a framework.

Oxidizer drainage is modeled using a pressure-driven formulation consistent with established nitrous oxide tank dynamics models [9, 10]. Solid-fuel regression is represented through a flux-based internal ballistics relation coupled to evolving port geometry [1, 2], enabling continuous tracking of fuel mass loss and grain growth. Oxidizer slosh is incorporated using a lumped-parameter model that approximates the distributed fluid motion with a small number of discrete dynamic states [5, 11], enabling acceleration-dependent mass redistribution to influence vehicle mass properties. These components are coupled through shared state variables within a variable-mass rigid-body formulation [6, 8], enabling direct prediction of time-varying total mass, COM, and MOI throughout the burn.

The proposed framework embeds internal propellant evolution directly within vehicle dynamics, enabling coupled propulsion–flight simulation with computational efficiency. It is demonstrated on a 1000-N hybrid VTVL lander developed by Propulsive Landers at Georgia Tech. The vehicle uses a pressure-fed nitrous oxide system, a paraffin–ABS fuel grain, and thrust vector control (TVC) for sustained attitude authority during ascent and powered descent. Oxidizer drainage and fuel port growth continuously alter internal mass distribution throughout flight.

*Undergraduate Student, Woodruff School of Mechanical Engineering, Atlanta, GA, 30332, AIAA University Student.
†Undergraduate Student, Guggenheim School of Aerospace Engineering, Atlanta, GA, 30332, AIAA University Student.
‡Undergraduate Student, Georgia Tech College of Computing, Atlanta, GA, 30332, AIAA University Student.

These variations shift center of mass and modify moment of inertia, directly affecting thrust-vector control effectiveness and rotational response. Accurate prediction of time-varying COM and MOI is therefore required to characterize vehicle dynamics during hover and descent.

II. Methodology

A. Regression Law and Analytical Port Evolution

Regression rate $\dot{r}$ defines the growth of the solid-fuel port radius during burn and directly sets fuel mass depletion, COM shift, and inertia variation. Hybrid regression is commonly modeled using the Marxman mass-flux power law (1963), relating regression rate to oxidizer mass flux [1]. This reduced-order relation captures transient port growth without resolving detailed combustion or boundary-layer physics, making it suitable for system-level analysis.

Paraffin differs from traditional polymeric fuels by exhibiting liquefying behavior that enhances regression through melt-layer droplet entrainment. Experimental studies, including work by Brian Cantwell and collaborators, show that a low-viscosity molten layer forms, becomes shear-unstable, and ejects droplets into the core flow, increasing regression beyond diffusion-limited predictions. Despite this mechanism, paraffin regression remains well represented by the classical flux-based power law with empirically calibrated coefficients reflecting entrainment-dominated behavior in paraffin–nitrous oxide systems. Fuel regression is modeled using the classical Marxman mass-flux power law,

$$\dot{r} = aG_o^n, \tag{1}$$

where $\dot{r}$ is the radial regression rate, G_o is oxidizer mass flux, and a and n are empirically calibrated coefficients for paraffin–nitrous oxide systems.

For a grain containing N identical cylindrical ports of radius R, and oxidizer mass flow rate $\dot{m}_o$, oxidizer mass flux is

$$G_o = \frac{\dot{m}_o}{\pi N R^2}. \tag{2}$$

Substituting Eq. (2) into Eq. (1) gives:

$$\dot{R} = a\left(\frac{\dot{m}_o}{\pi N R^2}\right)^n. \tag{3}$$

Assuming constant oxidizer mass flow rate, Eq. (3) can be integrated analytically to yield the port radius evolution

$$R(t) = \left[a(2n+1)\left(\frac{\dot{m}_o}{\pi N}\right)^n t + R_i^{2n+1}\right]^{\frac{1}{2n+1}}, \tag{4}$$

where R_i is the initial port radius.

This shows a nonlinear time-dependent port growth governed by the regression exponent n. Increasing radius reduces oxidizer mass flux by $G_o \propto R^{-2}$ and introduces geometric feedback that moderates regression over time.

1. Fuel Mass Flow and Remaining Mass

The instantaneous fuel mass flow rate with fuel density ρ_f and grain length L is

$$\dot{m}_f = 2\pi^{1-n}\rho_f L a \dot{m}_o^n R^{1-2n}. \tag{5}$$

The total remaining fuel mass follows from grain geometry. For N ports,

$$m_f(t) = \pi N \rho_f L\left[R(t)^2 - R_i^2\right]. \tag{6}$$

Substituting Eq. (4) provides a fully analytical expression for fuel mass evolution under constant oxidizer flow,

$$m_f(t) = \pi N \rho_f L\left\{\left[a(2n+1)\left(\frac{\dot{m}_o}{\pi N}\right)^n t + R_i^{2n+1}\right]^{\frac{2}{2n+1}} - R_i^2\right\}. \tag{7}$$

2. Coupling to Feed-System Model

In the present study, $\dot{m}_o$ is not constant but provided by the thrust-commanded oxidizer mass flow rate solver. Therefore, to predict the changing port diameter, Eq. (3) is applied over small time steps where $\dot{m}_o(t)$ can be modeled as constant. The evolving port radius and fuel mass are subsequently used to compute the time-varying vehicle center of mass and moment of inertia.

B. Thrust-Commanded Mass Flow Rate Solver

To couple propulsion and vehicle dynamics, the model takes in a commanded thrust T_{cmd}, the required oxidizer mass flow rate $\dot{m}_o$ is determined at each timestep. A discrete sweep of candidate oxidizer mass flow rates,

$$\dot{m}_o \in [0.001,\ 0.560] \text{ kg/s}, \tag{8}$$

is evaluated. For each candidate, fuel regression is computed using Eq. (4), yielding $\dot{m}_f$, mixture ratio O/F, and total mass flow rate

$$\dot{m}_{tot} = \dot{m}_o + \dot{m}_f. \tag{9}$$

Propulsion performance parameters $I_{sp}(\text{O/F})$ and $C^*(\text{O/F})$ are obtained from polynomial fits to precomputed NASA CEARun equilibrium data. Thrust is evaluated as

$$T(\dot{m}_o) = I_{sp}(\text{O/F})\,\dot{m}_{tot}, \tag{10}$$

and the $\dot{m}_o$ minimizing $|T - T_{cmd}|$ is selected.

Chamber pressure follows from

$$P_c = \frac{\dot{m}_{tot} C^*(\text{O/F}) \eta_{c^*}}{A_t C_d}. \tag{11}$$

The selected $\dot{m}_o$ is passed to the oxidizer drain model, and all propellant states are updated for the next timestep.

1. Assumptions and Limitations

- I_{sp} and C^* are derived from equilibrium CEA data and neglect pressure-coupled efficiency variation and non-equilibrium effects.
- Fuel regression uses an empirical mass-flux power law with constant coefficients a and n.
- The discrete $\dot{m}_o$ sweep introduces bounded numerical resolution error.

C. Nitrogen Pressurization and Reaction Control System Model

High-pressure gaseous nitrogen maintains the oxidizer run tank at 65 bar and supplies a cold-gas RCS. Because nitrogen mass is small relative to total vehicle mass, a reduced-order mass-accounting approach is adopted.

Each 5 N RCS thruster has mass flow estimated by

$$\dot{m} = \frac{T}{I_{sp} g_0}, \tag{12}$$

using $I_{sp} = 60$–75 s. When active, paired thrusters subtract twice this mass flow from nitrogen inventory.

Run tank ullage volume is computed from remaining nitrous mass assuming 15% initial ullage and constant nitrous density at 65 bar. Nitrogen mass is

$$m_{N_2,run}(t) = \rho_{N_2}(65 \text{ bar}, T_{tank}) V_{N_2}(t), \tag{13}$$

with density obtained from isobaric NIST data. Total nitrogen mass is updated each timestep by accounting for RCS consumption and ullage recomputation.

1. Assumptions and Limitations

- Nitrogen is assumed at uniform tank temperature and constant regulated pressure.
- Detailed regulator dynamics and supercritical blowdown effects are not modeled.

D. Oxidizer Drainage Model Overview

The feed system comprises a nitrous oxide tank, a throttling valve, and a showerhead injector feeding the combustion chamber. The drainage model takes the required injector mass flow rate, solves for the intermediate injector inlet pressure, then determines the effective valve area and corresponding opening angle needed to achieve that flow.

In general, two coupled models govern self-pressurizing propellant drainage: a tank-emptying model that tracks tank state evolution as mass is withdrawn, and a mass flow model that computes chamber inflow from upstream conditions, which then updates the tank state. [14].

To improve thrust controllability, the system uses steady external pressurization with gaseous nitrogen instead of nitrous oxide self-pressurization. This suppresses internal saturation dynamics and maintains nitrous oxide as a stable subcooled liquid. Upstream tank properties therefore remain constant inputs to the mass flow model, removing the need for a tank-emptying model. The configuration follows a three-state oxidizer feed architecture. [15]:

State 1: Tank fluid upstream of the valve with pressure, temperature, specific enthalpy (P_1, T_1, h_1).
State 2: Intermediate pressure downstream of the valve and upstream of the injector with (P_2, T_2, h_2).
State 3: Injector exit at chamber pressure with (P_3, T_3, h_3).

Nitrous oxide properties are obtained from NIST tables [16, 17]: Subcooled liquid enthalpy at the tank is h_1 (from isobaric data at T_1); saturation properties across the downstream pressure provide saturated liquid enthalpy $h_L(P)$, saturated vapor enthalpy $h_V(P)$, saturated liquid density $\rho_L(P)$, and saturated vapor density $\rho_V(P)$ with interpolation at each evaluated pressure.

1. Determination of Intermediate Pressure P_2

Injector mass flow is modeled using the Dyer formulation due to its reliability in predicting two-phase flow through throttling components.

The oxidizer mass flow rate required to meet the target thrust is obtained from the previously defined propulsion relation. The tank contains subcooled liquid with enthalpy evaluated at the tank state, and flow through the valve and injector is assumed isenthalpic.

If downstream pressure drop induces flashing, vapor quality is determined from the upstream enthalpy relative to saturated liquid and vapor values at the local pressure. Mixture enthalpy and density are then evaluated along the saturation line.

Dyer Model [14]:

$$\dot{m}(P_2) = \left(1 - \frac{1}{1+\kappa}\right)\dot{m}_{SPI} + \left(\frac{1}{1+\kappa}\right)\dot{m}_{HEM}, \tag{14}$$

The intermediate pressure P_2 is found numerically by solving

$$f(P_2) = \dot{m}(P_2) - \dot{m}_{\text{req}}, \tag{15}$$

where $\dot{m}(P_2)$ is the Dyer model mass flow for a guessed P_2. Trial values of P_2 are chosen within $P_3 < P_2 < P_1$ with interpolated saturation properties, and a root-bracketing method iteratively adjusts P_2 until $f(P_2) = 0$, ensuring the injector flow matches the required mass flow.

2. Determination of Effective Valve Area

Once P_2 is determined, a unit flow capacity $\Phi(P_1, P_2)$ is computed using pressure drop $P_1 \to P_2$, which is scales linearly with discharge coefficient and valve area:

$$A_{valve} = \frac{\dot{m}_{req}}{C_{d,valve}\Phi(P_1, P_2)}. \tag{16}$$

3. Throttle Valve Opening Angle

To control the valve opening, the required A_{valve} must be converted to the corresponding θ_{valve}, fully closed to fully opened. Our system uses a ½-inch ball valve with a 60° V-port [18]. The valve's throat plane coincides with the mid-seat plane containing the ball's axis of rotation. Thus, A_{valve} is identical to the portion of the throat plane enclosed by the ball valve as it rotates.

To establish $\theta_{valve}(A_{valve})$, a motion study was performed on the manufacturer-provided valve CAD model. The study captured an orthographic video of the color-coded throat plane at 3100×2000 resolution and 120 FPS, with the valve rotating at 1 RPM (6°/s).

The complete θ_{valve} interval was found between the time stamps at which the maximum (fully open) and zero (fully closed) A_{valve}-representing pixel counts are detected. Combined with the maximum A_{valve} measured from the model, this yielded a maximum θ_{valve} range. Intermediate pixel counts were then proportionally mapped to the corresponding A_{valve} and θ_{valve} values.

A shape-preserving piecewise cubic Hermite interpolation was then applied to generate a continuous and unique $\theta_{valve}(A_{valve})$ mapping, accurate to ±0.025°. This enables highly sensitive, near-instantaneous valve control when integrated with in-flight dynamics programming.

E. Reduced-Order Oxidizer Slosh Model

Lateral accelerations from wind disturbances, thrust-vector control (TVC) (Thrust Vector Control), and attitude transients can excite oxidizer motion in a partially filled tank. To support real-time mass-property prediction, slosh is modeled using a reduced-order equivalent mechanical representation that outputs the integrated body-frame disturbance force without resolving the internal flow field [5, 11, 19]. A single lateral mode is retained in each transverse direction, with rigid walls, incompressible liquid, and amplitude-dependent restoring behavior represented using a Duffing-type cubic stiffness [19, 20].

1. Excitation and first-mode parameterization

At each timestep, the model is driven by the effective lateral excitation (specific force) in the body frame, formed by combining the commanded/estimated translational acceleration with gravity projected into the body axes. The instantaneous fill height is computed from the remaining liquid mass $m_\ell(t)$ as

$$h(t) = \frac{m_\ell(t)}{\rho_\ell \pi R^2}, \tag{17}$$

and the first lateral slosh-mode frequency for a finite-depth cylindrical tank is approximated using linear potential-flow theory as [5, 19]

$$\omega_n(t) = \sqrt{g\left(\frac{1.841}{R}\right)\tanh\left(\frac{1.841\,h(t)}{R}\right)}. \tag{18}$$

An optional tuning factor may be applied as $\omega(t) = \omega_{\text{scale}}\omega_n(t)$. The participating (effective) slosh mass is modeled as $m_{\text{eq}}(t) = \frac{1}{2}m_{\text{frac}}m_\ell(t)$, consistent with common first-mode momentum-exchange approximations [11].

2. Duffing oscillator and force-level output

For each lateral axis (applied independently in x and y), the slosh coordinate is modeled as a base-excited Duffing oscillator,

$$m_{\text{eq}}\ddot{x} + c_{\text{lin}}\dot{x} + m_{\text{eq}}\omega^2 x + \alpha x^3 = -m_{\text{eq}}a^*, \tag{19}$$

where a^* is the corresponding effective lateral excitation. The disturbance force applied to the vehicle is computed from the restoring and damping contributions,

$$F = c_{\text{lin}}\dot{x} + m_{\text{eq}}\omega^2 x + \alpha x^3, \tag{20}$$

yielding $F_s = [F_x \quad F_y \quad 0]^T$ for direct use in rigid-body simulation and guidance, navigation, and control (GNC) (Guidance, Navigation, and Control) analyses.

F. Center of Mass and Moment of Inertia Formulation

Center of mass (COM) and moment of inertia (MOI) evolution determine the vehicle's rigid-body response during burn. Because this study focuses on internal mass redistribution in a hybrid rocket, accurate tracking of these quantities is required to assess stability margins and control authority. As oxidizer depletes, fuel regresses, and pressurant redistributes, total mass and its distribution change continuously, driving COM migration and time-varying inertia.

Rather than assuming fixed or lumped properties, the model recomputes system-level COM and MOI over time by coupling propellant depletion with pre-characterized dry structural properties. This reduced-order formulation maintains rigid-body fidelity while remaining computationally efficient for flight dynamics integration.

G. Dry Mass Characterization from CAD

Dry structural mass properties were extracted from SolidWorks using detailed CAD models of each major subsystem, including the frame, landing gear, engine assembly, and tank structures. Material properties consistent with the as-built configuration were assigned to each component.

For each subsystem, SolidWorks provided total mass, center-of-mass location, and inertia tensor relative to a common vehicle reference frame. These values were exported and assembled into a composite rigid-body model.

The total dry center of mass was computed using the mass-weighted relation

$$\mathbf{r}_{COM,dry} = \frac{\sum_i m_i \mathbf{r}_i}{\sum_i m_i}, \tag{21}$$

where m_i and $\mathbf{r}_i$ are the mass and centroid location of each component.

The total dry inertia tensor about the vehicle origin was obtained using the parallel-axis theorem,

$$\mathbf{I}_{total} = \sum_i \left(\mathbf{I}_{i,c} + m_i \left[(\mathbf{d}_i \cdot \mathbf{d}_i)\mathbf{I} - \mathbf{d}_i \mathbf{d}_i^T \right] \right), \tag{22}$$

where $\mathbf{I}_{i,c}$ is the inertia tensor of component i about its centroid and $\mathbf{d}_i$ is the displacement vector from the component centroid to the vehicle reference origin.

These dry properties establish the baseline configuration. Time-dependent propellant and pressurant mass contributions are subsequently superimposed using the oxidizer drain and fuel regression models described in previous sections.

H. Full Dynamics Simulation

To maintain stable hover and descent, the lander must be able to balance using the TVC while experiencing mass loss and internal mass redistribution due to propellant burn. As a result, center of mass (CoM) and moment of inertia (MoI) change, significantly affecting the control authority of VTVL vehicles such as this lander. By coupling mass evolution and thermodynamics to the Newton-Euler equations of motion, a more accurate understanding of the dynamics of the vehicle can be obtained allowing for more accurate sensor fusion, control, and guidance algorithms can be developed.

A fully-coupled 6-degree-of-freedom (6-DoF) dynamics model is created in Rust to provide an accurate simulation of the vehicle dynamics and mass evolution. Typical dynamics simulations do not take into account changing CoM or MoI [21, 22]. This makes these models unable to couple the fluid and thermodynamics to the mass and moment of inertia. To model vehicle dynamics with the most accuracy, these effects must be taken into account.

Physics are updated via Euler integration at a rate of 0.02 seconds, along with the mass values of the tanks and fuel grain, as well as the regression for the fuel grain and nozzle throat. Mass flow across the throttle valve and the resulting chamber pressure and thrust are also modeled at each time step. The CoM and MoI are recalculated at each timestep based off the mass of each tank, percentage of fill of each tank, and the mass of the TVC module.

In addition to physics simulations, the dynamics model simulates controls for the vehicle. The simulation runs through a flight profile of an ascent to 50 meters, a 10 second hover, then a descent back down to the ground. Control is provided by model predictive control (MPC), while navigation is provided by an implementation of lossless convexification (LCvx). LCvx provides full trajectory guidance, but neglects angular dynamics since angular dynamics evolves much more quickly than translational dynamics. MPC focuses on optimizing control sequences over a short period of time, providing exact control outputs at each step.

III. Results and Discussion

This section presents results from the fully coupled propulsion–mass evolution simulation described in Section III. All quantities were computed in real time using the thrust-commanded mass flow solver, oxidizer drain model, regression law, nitrogen accounting model, and time-varying COM/MOI formulation. Representative time histories are shown in the simulation output plots .

A. Mass Evolution

Time histories of fuel mass, nitrous oxide mass, and total vehicle mass are shown in Fig. 1. Fuel mass decreases nonlinearly throughout the burn due to the coupled regression–flux relation. Early in the burn, elevated oxidizer mass flux produces higher regression rates. As port radius increases, oxidizer mass flux decreases according to $G_o \propto R^{-2}$, moderating regression and introducing curvature in the fuel mass profile. This behavior is consistent with the analytical port growth solution derived in Section III and demonstrates proper implementation of the flux-based regression model.

Nitrous oxide mass depletion follows the thrust-commanded oxidizer mass flow rate solver. Unlike fuel regression, which is geometry-driven, oxidizer depletion is directly governed by the inverse thrust calculation. Slope changes in the oxidizer mass curve correspond to throttle transitions observed in Fig. III.D. During reduced-thrust segments, oxidizer mass depletion rate decreases, then increases again when thrust is commanded higher. This confirms tight coupling between thrust demand and feed-system response.

Total vehicle mass decreases monotonically throughout the burn. The combined nonlinear regression and commanded oxidizer depletion produce a smooth, continuous total mass trajectory without numerical discontinuities, indicating stable timestep integration.

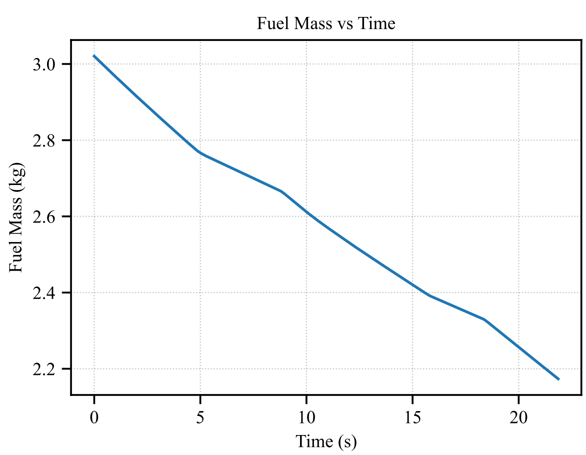

(a) Fuel mass vs. time.

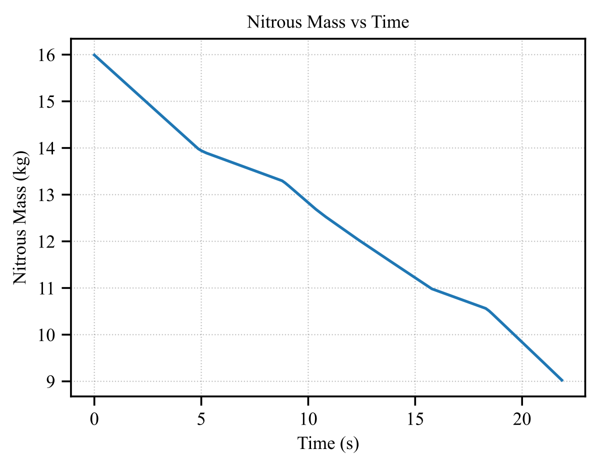

(b) Nitrous oxide mass vs. time.

Fig. 1 Propellant mass evolution during the burn.

B. Nitrogen Redistribution and Pressurization Effects

Nitrogen storage and run-tank mass histories are shown in Fig. 2. As nitrous oxide mass decreases, liquid volume contracts and ullage volume increases. To maintain the regulated 65 bar condition, nitrogen mass within the run tank increases over time. This increase is balanced by a corresponding decrease in storage tank nitrogen mass.

The redistribution remains smooth and gradual, validating the reduced-order mass accounting approach adopted in Section III.C. The magnitude of nitrogen mass transfer is small relative to total vehicle mass but non-negligible in center-of-mass calculations due to axial separation between storage and run tanks. The results confirm that first-order pressurization effects can be captured without modeling supercritical blowdown dynamics.

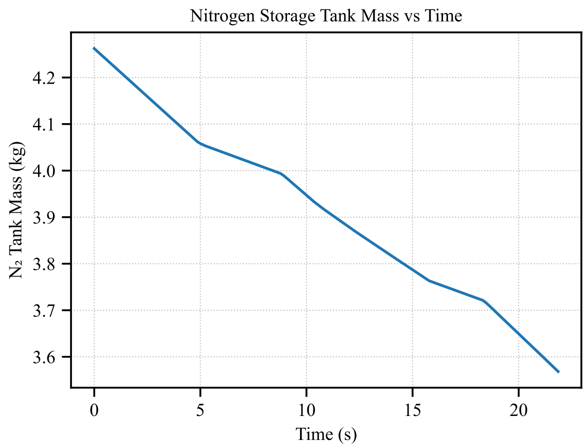

(a) Nitrogen storage tank mass vs. time.

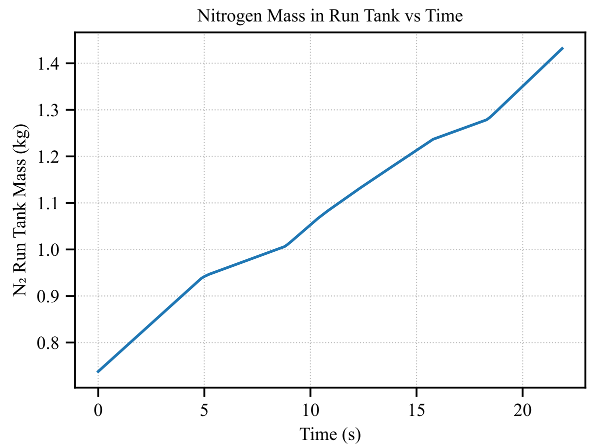

(b) Nitrogen mass in run tank vs. time.

Fig. 2 Nitrogen mass redistribution during the burn. As oxidizer volume decreases, ullage volume increases, resulting in nitrogen transfer from storage to the run tank to maintain regulated pressure.

C. Center of Mass and Moment of Inertia

The time evolution of vehicle center-of-mass (COM) and principal moments of inertia (MOI) is shown in Fig. 3, with both recomputed at each timestep using the composite rigid-body formulation described in Section III to couple dry structure with time-varying propellant and pressurant masses. COM migration occurs primarily along the longitudinal axis as nitrous oxide is depleted and fuel regresses inward, producing a smooth, monotonic axial shift with minor slope changes corresponding to throttle transitions in Fig. III.D, while lateral components remain near zero under symmetric operation. Although the absolute COM displacement is modest, it alters the thrust-vector control lever arm and therefore the torque generated for a given gimbal input in a VTVL architecture. Principal moments of inertia decrease continuously due to cumulative mass loss and inward radial contraction of the fuel grain, modifying rotational response according to $\tau = I\alpha$ such that decreasing inertia increases angular acceleration for fixed torque; neglecting inertia evolution would therefore yield progressively inaccurate attitude predictions. The smooth COM and MOI trajectories confirm numerical stability of the unified mass-evolution framework and its suitability for real-time 6-DoF simulation.

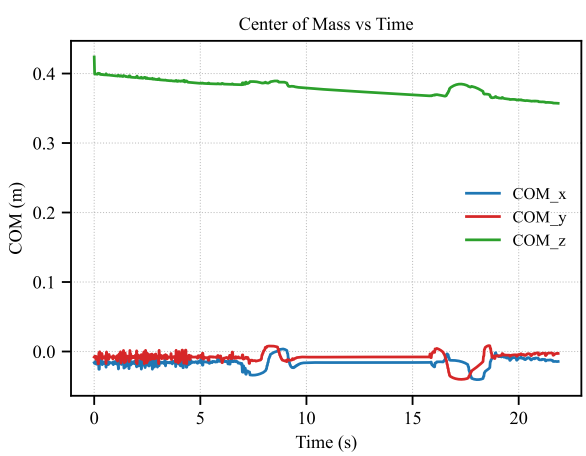

(a) Center-of-mass components vs. time.

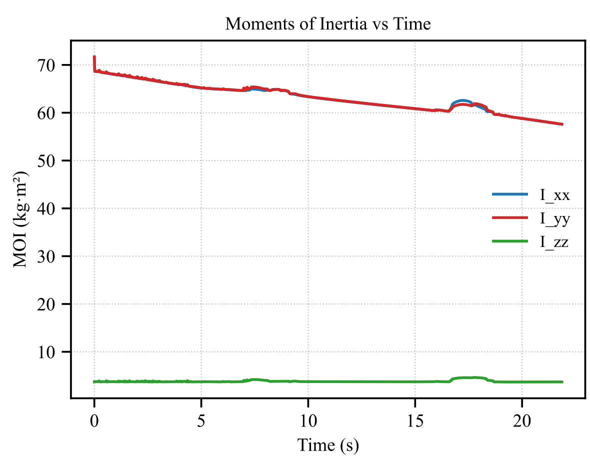

(b) Principal moments of inertia vs. time.

Fig. 3 Time-varying mass properties during the burn.

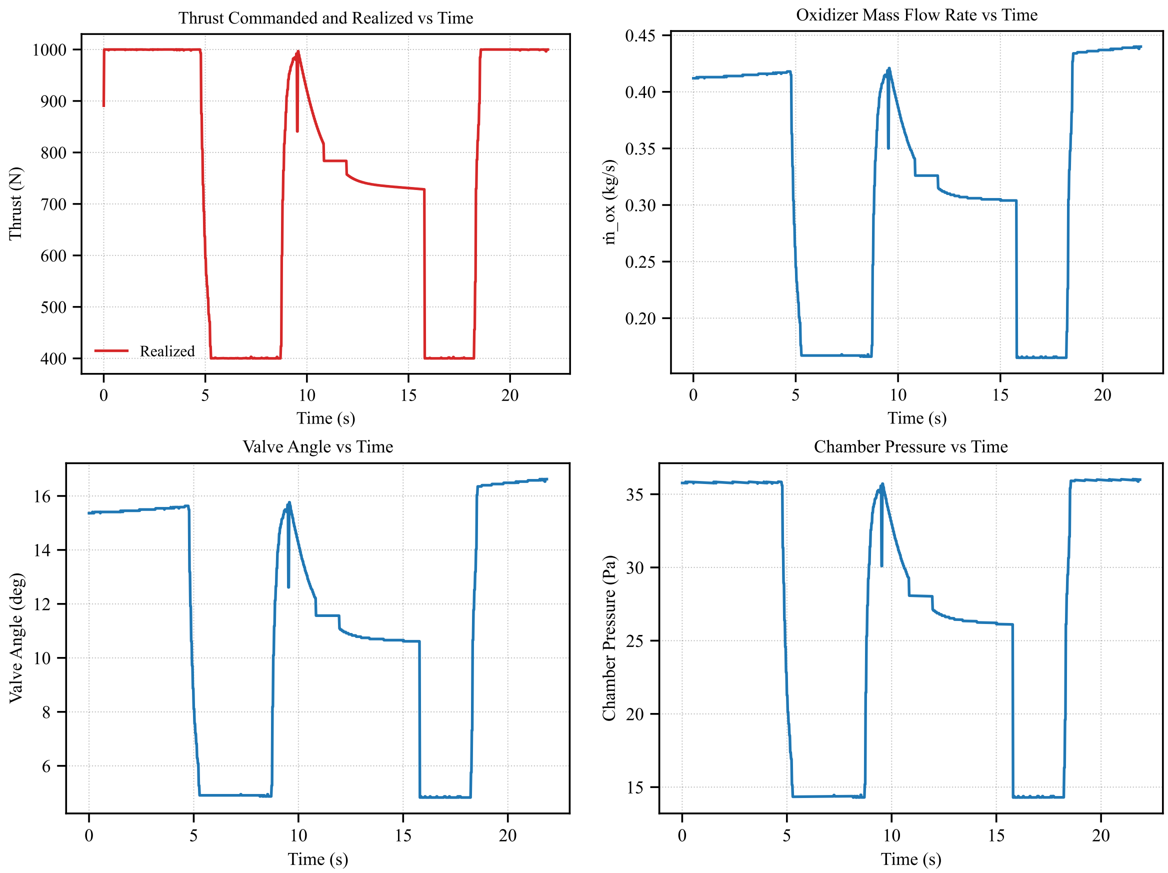

Fig. 4 Propulsion state histories during throttled burn.

D. Propulsion State Consistency and Solver Stability

Propulsion state histories are shown in Fig. III.D. Commanded and realized thrust track closely throughout ascent, hover, and descent phases. The discrete oxidizer mass flow sweep achieves accurate thrust matching without requiring iterative equilibrium combustion solvers.

Oxidizer mass flow rate varies consistently with throttle transitions, and valve angle adjusts accordingly to generate the required intermediate pressure drop. Chamber pressure evolves in direct relation to total mass flow via the characteristic velocity formulation. Transitions remain smooth and stable, with no oscillatory behavior or solver divergence observed.

The absence of numerical discontinuities across thrust, mass flow, valve angle, chamber pressure, COM, and MOI histories confirms that the reduced-order framework remains stable under dynamic throttling conditions. Coupling between regression, feed system modeling, pressurization accounting, and rigid-body mass property recomputation is maintained throughout the simulated burn.

E. Implications for VTVL Hybrid Architectures

The results demonstrate that internal mass redistribution in a throttled hybrid rocket produces continuous, coupled variation in total mass, center of mass, and moment of inertia. While each individual variation may appear modest in isolation, their combined effect directly alters translational and rotational vehicle response during powered flight.

Embedding regression physics, oxidizer drainage, nitrogen redistribution, and inertia recomputation within a unified framework enables real-time prediction of mass property evolution suitable for guidance and control simulation. This capability is particularly relevant for VTVL systems where thrust-vector control authority and stability margins depend directly on evolving internal mass distribution.

IV. Conclusion

A reduced-order, analytically driven framework was developed to predict hybrid-rocket in-flight internal mass evolution by coupling oxidizer outflow, solid-fuel regression, pressurant accounting, and acceleration-driven slosh within a single system-level simulation. The objective was not high-fidelity prediction of detailed combustion or internal flow fields, nor maximum pointwise accuracy of any individual submodel in isolation, but rather a tractable representation of the coupled mechanisms that jointly govern time-varying mass properties relevant to guidance and control. By enforcing these interactions in one consistent formulation, the model functions as a system-level "coupling engine" that exposes how changes in one subsystem (e.g., throttling, regression-driven port growth, ullage expansion, or acceleration history) propagate into the others and ultimately shape total mass, center of mass (COM), and moment of inertia (MOI). Implemented within a fully coupled 6-DoF simulation, the formulation produces continuous updates of mass properties throughout a representative VTVL ascent–hover–descent profile.

Simulation results show that propellant depletion and redistribution produce smooth but persistent mass-property variation over the burn. The thrust-commanded mass-flow solver maintains close thrust tracking while simultaneously updating mixture ratio, chamber pressure, and regression-driven port growth; this enables propulsion consistency without requiring runtime equilibrium calculations and, importantly, makes the internal mass evolution responsive to commanded thrust history rather than prescribed a priori. Oxidizer mass history follows throttling behavior, while the fuel mass evolution remains inherently nonlinear due to oxidizer-flux feedback as the port expands. These coupled mechanisms directly drive the observed axial COM migration and the monotonic reduction of the principal moments of inertia, reflecting both decreasing propellant mass and contraction of radial mass distribution as regression proceeds. Pressurant mass redistribution (storage-to-run-tank transfer as ullage volume increases) is also captured within the same accounting structure, closing the loop between volume change, pressurant demand, and time-varying internal inventory. Finally, the reduced-order slosh model supplies acceleration-dependent disturbance forces and transient internal mass motion consistent with a first-mode lumped-parameter representation, enabling the simulation to reflect how trajectory-driven accelerations can alter effective internal loading and mass distribution even when total propellant mass changes smoothly.

The primary implication is that hybrid VTVL vehicles experience continuously evolving mass properties during powered flight, and these changes directly modify thrust-vector control effectiveness and rotational response. Consequently, control architectures that assume fixed COM/MOI risk systematic mismatch in predicted dynamics, particularly during hover and descent where attitude authority margins can be tight. In this sense, the main value of the presented approach is not that it replaces higher-fidelity combustion, feed-system, or CFD-based slosh tools, but that it makes the interdependencies between propulsion, pressurization, and internal fluid motion explicit within a computationally efficient loop—allowing designers to identify which couplings dominate, when they matter in the trajectory, and what they imply for control allocation, gain scheduling, and robustness.

The current formulation remains limited by its reduced-order assumptions: regression is represented by an empirical mass-flux law with fixed coefficients; feed-system modeling assumes quasi-steady, one-dimensional behavior with constant discharge parameters under regulated tank pressure; and the slosh representation retains only the first lateral mode and omits multi-mode, rotational coupling, and complex free-surface effects. Future work should focus on validation against static-fire or tethered-flight datasets, refinement of throttle-transient regression and injector parameterizations, extension of slosh to multi-mode or three-dimensional tank representations, and uncertainty bounding via timestep and model-sensitivity studies. Even as those fidelity improvements are pursued, the framework's role as a coupling-centric tool remains: it provides a practical way to explore how uncertain or simplified submodels interact at the vehicle level, and to translate those interactions into actionable guidance and control design decisions that explicitly account for time-varying hybrid-rocket mass properties.

References

[1] Sutton, G. P., and Biblarz, O., *Rocket Propulsion Elements*, 9$^{\text{th}}$ ed., Wiley, Hoboken, NJ, 2017.

[2] Karabeyoglu, A., Zilliac, G., and Cantwell, B., "Transient Modeling of Hybrid Rocket Internal Ballistics," *Journal of Propulsion and Power*, Vol. 20, No. 6, 2004, pp. 1107–1116.

[3] Karabeyoglu, A., Altman, D., and Cantwell, B., "Combustion of Liquefying Hybrid Propellants: Part 1, General Theory," *Journal of Propulsion and Power*, Vol. 18, No. 3, 2002, pp. 610–620.

[4] Meriam, J. L., and Kraige, L. G., *Engineering Mechanics: Dynamics*, 8$^{\text{th}}$ ed., Wiley, 2016.

[5] Abramson, H. N., "The Dynamic Behavior of Liquids in Moving Containers," Tech. Rep. NASA SP-106, NASA, 1966.

[6] Kane, T. R., and Levinson, D. A., "Equations of Motion for Variable Mass Systems," *Journal of Applied Mechanics*, Vol. 49, 1982, pp. 927–931.

[7] Cicolani, L. S., "Global Modeling of Propellant Slosh for Launch Vehicles," *Journal of Guidance, Control, and Dynamics*, Vol. 13, No. 5, 1990.

[8] Wie, B., "Effects of Mass Variation on Launch Vehicle Attitude Dynamics," *Journal of Guidance, Control, and Dynamics*, 1989.

[9] Zilliac, G. G., and Karabeyoglu, A., "Modeling of Self-Pressurizing Propellant Tank Dynamics," *39th AIAA/ASME/SAE/ASEE Joint Propulsion Conference*, 2003.

[10] Waxman, B. S., and Karabeyoglu, A., "Modeling of Nitrous Oxide Tank Blowdown for Hybrid Rocket Applications," *AIAA Propulsion and Energy Conference*, 2011.

[11] Dodge, F. T., "The New Dynamic Behavior of Liquids in Moving Containers," Tech. rep., Southwest Research Institute, 2000.

[12] Lucia, D. J., Beran, P. S., and Silva, W. A., "Reduced-Order Modeling: New Approaches for Computational Physics," *Progress in Aerospace Sciences*, Vol. 40, 2004, pp. 51–117.

[13] Rowley, C. W., and Dawson, S. T. M., "Model Reduction for Flow Analysis and Control," *Annual Review of Fluid Mechanics*, Vol. 49, 2017, pp. 387–417.

[14] Sarritzu, A., Pesante, M. R., La Luna, S., and Pasini, A., "Review and Perspectives of 'Green' Self-Pressurizing Propellants for In-Space Propulsion and Their Applicability to Orbital Stages," *AIAA SciTech 2024 Forum*, 2024. https://doi.org/10.2514/6.2024-1791, aIAA 2024-1791.

[15] Peterson, Z. W., Eilers, S. D., and Whitmore, S. A., "Closed-Loop Thrust and Pressure Profile Throttling of a Nitrous-Oxide HTPB Hybrid Rocket Motor," *AIAA/ASME/SAE/ASEE Joint Propulsion Conference & Exhibit*, 2012. https://doi.org/10.2514/6.2012-4200, URL https://arc.aiaa.org/doi/10.2514/6.2012-4200, aIAA 2012-4200.

[16] National Institute of Standards and Technology (NIST), "Isobaric Properties for Dinitrogen Monoxide (Nitrous Oxide)," NIST Chemistry WebBook, SRD 69, ???? URL https://webbook.nist.gov/cgi/fluid.cgi?P=6.5&TLow=&THigh=&TInc=&Digits=5&ID=C10024972&Action=Load&Type=IsoBar&TUnit=K&PUnit=MPa&DUnit=mol%2Fl&HUnit=kJ%2Fmol&WUnit=m%2Fs&VisUnit=uPa*s&STUnit=N%2Fm&RefState=DEF, isobaric data at $P = 6.5000$ MPa.

[17] National Institute of Standards and Technology (NIST), "Saturation Properties for Dinitrogen Monoxide (Nitrous Oxide)," NIST Chemistry WebBook, SRD 69: Thermophysical Properties of Fluid Systems, n.d. URL https://webbook.nist.gov/cgi/fluid.cgi?TLow=&THigh=&TInc=&Digits=5&ID=C10024972&Action=Load&Type=SatP&TUnit=K&PUnit=MPa&DUnit=mol%2Fl&HUnit=kJ%2Fmol&WUnit=m%2Fs&VisUnit=uPa*s&STUnit=N%2Fm&RefState=DEF.

[18] Valworx, "1/2" V-Port 3-Piece Stainless Ball Valve 60°," , n.d. URL https://www.valworx.com/v-port-3-piece-stainless-ball-valve-12-60deg, product page.

[19] Ibrahim, R. A., *Liquid Sloshing Dynamics: Theory and Applications*, Cambridge University Press, 2005.

[20] Faltinsen, O. M., and Timokha, A. N., *Sloshing*, Cambridge University Press, 2009.

[21] Reynolds, T. P., Szmuk, M., Malyuta, D., Mesbahi, M., Açıkmeşe, B., and Carson III, J. M., "Dual Quaternion-Based Powered Descent Guidance with State-Triggered Constraints," *Journal of Guidance, Control, and Dynamics*, Vol. 43, No. 9, 2020, pp. 1584–1599. https://doi.org/10.2514/1.G004536.

[22] Sagliano, M., Heidecker, A., Macés Hernández, J. A., Farì, S., Schlotterer, M., Woicke, S., Seelbinder, D., and Dumont, E., "Onboard Guidance for Reusable Rockets: Aerodynamic Descent and Powered Landing," *AIAA Scitech 2021 Forum*, 2021. https://doi.org/10.2514/6.2021-0862.